

# Hapten-Decorated DNA Nanostructures Decipher the Antigen-Mediated Spatial Organization of Antibodies Involved in Mast Cell Activation

Leonie Schneider, Kersten S. Rabe, Carmen M. Domínguez, and Christof M. Niemeyer\*



Cite This: *ACS Nano* 2023, 17, 6719–6730



Read Online

ACCESS |



Metrics & More

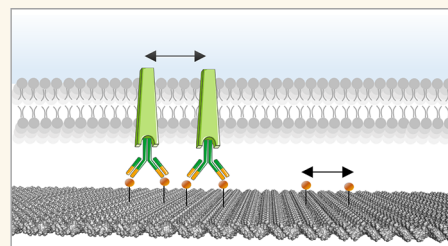


Article Recommendations



Supporting Information

**ABSTRACT:** The immunological response of mast cells is controlled by the multivalent binding of antigens to immunoglobulin E (IgE) antibodies bound to the high-affinity receptor FcεRI on the cell membrane surface. However, the spatial organization of antigen–antibody–receptor complexes at the nanometer scale and the structural constraints involved in the initial events at the cell surface are not yet fully understood. For example, it is unclear what influence the affinity and nanoscale distance between the binding partners involved have on the activation of mast cells to degranulate inflammatory mediators from storage granules. We report the use of DNA origami nanostructures (DON) functionalized with different arrangements of the haptenic 2,4-dinitrophenyl (DNP) ligand to generate multivalent artificial antigens with full control over valency and nanoscale ligand architecture. To investigate the spatial requirements for mast cell activation, the DNP–DON complexes were initially used in surface plasmon resonance (SPR) analysis to study the binding kinetics of isolated IgE under physiological conditions. The most stable binding was observed in a narrow window of approximately 16 nm spacing between haptens. In contrast, affinity studies with FcεRI-linked IgE antibodies on the surface of rat basophilic leukemia cells (RBL-2H3) indicated virtually no distance-dependent variations in the binding of the differently structured DNP–DON complexes but suggested a supramolecular oligovalent nature of the interaction. Finally, the use of DNP–DON complexes for mast cell activation revealed that antigen-directed tight assembly of antibody–receptor complexes is the critical factor for triggering degranulation, even more critical than ligand valence. Our study emphasizes the significance of DNA nanostructures for the study of fundamental biological processes.



**KEYWORDS:** DNA nanotechnology, DNA origami, cell activation, receptors, antibodies

## INTRODUCTION

The immune system of humans and animals has developed precise mechanisms to respond to infections caused by potentially harmful pathogens such as bacteria and viruses. Here, the spatial ligand presentation of foreign antigens, which are often highly repetitively organized at the nanoscale, plays an important role.<sup>1</sup> The immune system possesses the ability to recognize such previously encountered surface structures, also known as pathogen-associated molecular patterns (PAMPs).<sup>2</sup> The resulting strong immune response caused by these features has been successfully exploited within the development of vaccines, such as Hepatitis B virus (HBV)<sup>3</sup> or Human Papillomavirus (HPV).<sup>4</sup> However, it was found that ligand density or stoichiometry is not solely responsible for optimal signaling activation during cell regulation. Instead, the spatial organization of transmembrane receptors has increasingly emerged as a crucial component for cell effector function.<sup>5</sup>

Mast cells regulate immunoglobulin E (IgE)-mediated immunological responses by releasing several inflammatory mediators stored in granules. However, this biological mechanism can in fact lead to the initiation and development of autoimmunity and allergic diseases when the cell activation is overexaggerated or inappropriately triggered.<sup>6</sup> Initial signal transduction is induced through antibody–receptor and antibody–antigen binding events on the cell surface.<sup>7</sup> The spatial organization of IgE's high-affinity transmembrane receptor, FcεRI, into molecular cluster assemblies initiates a

Received: December 21, 2022

Accepted: March 7, 2023

Published: March 29, 2023



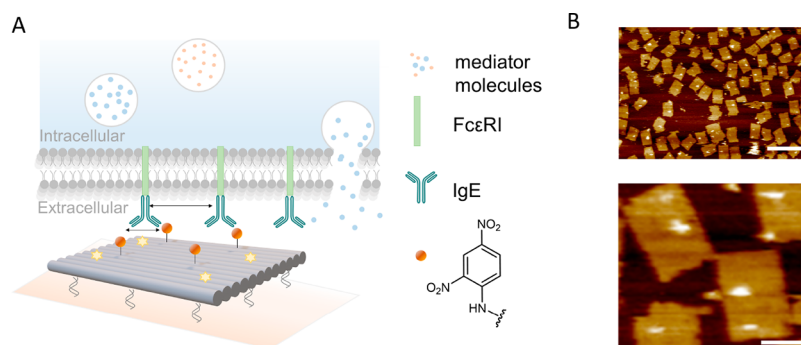


**Figure 1.** DNA origami nanostructures (DON) are used to present activating ligands to the surface of mast cells to enable investigation of antigen-mediated mast cell activation. (A) Schematic illustration of 2,4-dinitrophenyl (DNP, orange circles) hapten-decorated DON that contain protruding capture strands for immobilization on solid surfaces and fluorophores (yellow stars) for fluorescence microscopy analyses. Depending on the spatial nanoscale arrangement of DNP, immunoglobulin E (IgE) antibodies bound to the FcεRI transmembrane receptor of mast cells can bind to the DON at varying extents and trigger receptor clustering and degranulation of inflammatory mediators. (B) Atomic force microscopy (AFM) images of the DNP-decorated DON visualized through the attachment of immunoglobulin G (IgG) antibodies. Scale Bars: 300 nm (top) and 50 nm (bottom).

tyrosine kinase cascade which results in degranulation and *de novo* synthesis of bioactive compounds.<sup>8</sup> Receptor-clustering is mediated by multivalent recognition of antigenic structures by the antigen-binding fragments (Fab) of FcεRI-bound IgE antibodies on the cell surface.<sup>9</sup> In recent decades, several approaches have been pursued aiming to obtain a better understanding of the structural constraints in these initial binding events as well as the associated cellular signal regulation. Within this research, the spatial arrangement of antibody–receptor complexes directed by antigen binding has been an area of special interest.<sup>10</sup>

A well-established model system to investigate degranulation and early signaling pathways of mast cells is the Rat Basophilic Leukemia (RBL-2H3) cell line.<sup>11</sup> For this purpose, the cells can be sensitized with monoclonal IgE antibodies directed against a specific hapten, such as 2,4-dinitrophenol (DNP).<sup>12</sup> In previous studies multivalent hapten conjugates using a protein carrier were successfully used for initiation of RBL-2H3 cell activation, with DNP-modified bovine serum albumin being the most prominent one.<sup>13</sup> However, the nonspecific chemical coupling of hapten molecules to accessible lysine residues within the protein causes intrinsic heterogeneity in such conjugates. This means that no precise spatial arrangement of hapten molecules can be obtained with the consequence that hardly any studies on the spatial constraints of IgE–FcεRI complexes and IgE–hapten binding are possible. A more specific approach was pursued by Gieras *et al.*, who genetically engineered IgE epitopes of a grass pollen allergen in a myoglobin protein scaffold with varied stoichiometry and positions.<sup>14</sup> They were able to demonstrate that nearby epitopes caused higher cell activation than distantly placed epitopes with the same stoichiometry. However, the nonplanar folded protein structure makes precise distance prediction difficult. Furthermore, steric constraints of the protein environment may affect the affinity of FcεRI-bound IgE to the embedded epitopes.<sup>15</sup>

In contrast to multivalent hapten–protein conjugates, low-valency compounds such as bivalent DNP ligands with flexible spacers<sup>16</sup> and more rigid double-stranded (ds) DNA spacers<sup>17</sup> offered better spatial control but provided limited insight into the structural constraints of early cell signaling, due to little or no overall degranulation.<sup>16,18</sup> Furthermore, the intramolecular bivalent binding of two Fab fragments of a single antibody to

bivalent ligands with a certain distance ( $\sim 10$  nm) was found to inhibit efficient receptor clustering and degranulation.<sup>19</sup> Trimeric ligands of branched dsDNA caused higher levels of cellular response and revealed a distance-dependence in cell regulation for DNP distances between 5–13 nm.<sup>20</sup> Still, the significance of these reagents in terms of valency and distance was limited due to the flexibility of DNP ligands varying with the length of the branched dsDNA scaffold. Therefore, detailed analysis of ligand-induced FcεRI–IgE cross-linking that triggers effector cell degranulation still lacks a powerful molecular tool that allows variable ligand valency while maintaining precise control over the intermolecular binding distances at the nanoscale.

In recent years, Rothmund's scaffolded origami technique<sup>21</sup> has emerged as a promising tool for the study of biological processes, such as cell adhesion and activation.<sup>5,22–36</sup> DNA origami nanostructures (DON) can be used as molecular pegboards for presenting immobilized bioactive ligands to cells and tissues, thus enabling complete control over the number and spatial arrangement of ligands at the lower nanoscale. Here, we report on the use of DNP-decorated DON in order to investigate the spatial nanoscale tolerance for bivalent binding of anti-DNP IgE and anti-DNP IgG, as well as cell membrane-associated IgE antibodies. In addition, various nanoscale arrays with different hapten valencies were used to investigate the structural constraints of FcεRI–IgE complexes binding to multivalent antigens to initiate mast cell effector function. The results obtained shine light on the interplay of antigen, antibody, and receptor interactions in the cellular immune response.

## RESULTS AND DISCUSSION

To investigate the structural constraints on the initial binding events that are crucial for mast cell activation, we used a rectangular DON design with a size of  $70 \times 100$  nm<sup>2</sup>. The DON served as molecular pegboards for the nanometer-scale assembly of the small hapten 2,4-dinitrophenol (DNP), thereby creating multivalent and structurally defined ligand constructs (Figure 1). Additionally, the DON contained oligonucleotide strands protruding from the planar plane to enable immobilization on solid surfaces by DNA hybridization. Likewise, fluorophores were integrated into the DON scaffold for optical monitoring. For details of the design, see Figure S1.

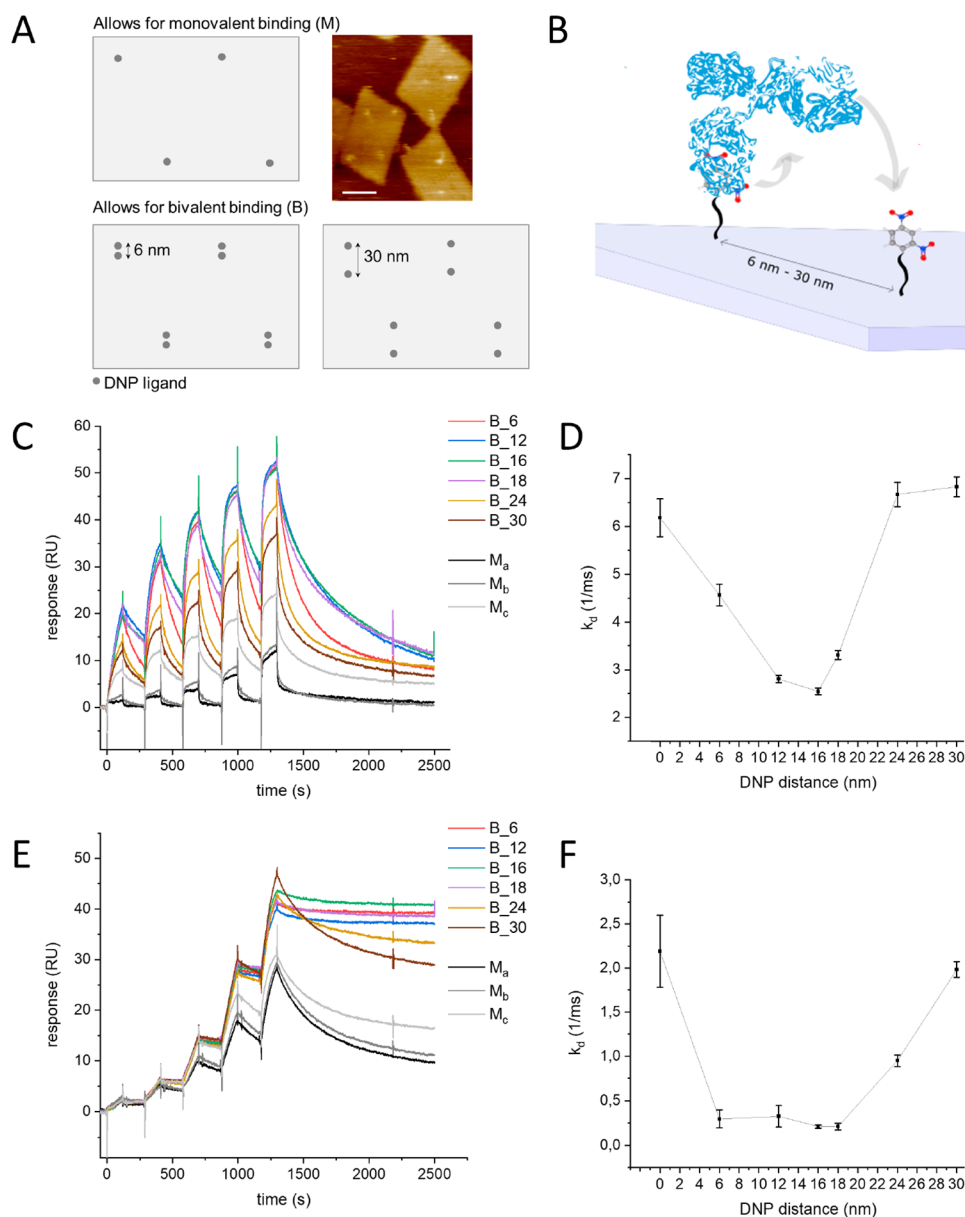


**Figure 2.** Investigation of the spatial tolerance of anti-DNP IgE and anti-DNP IgG for bivalent binding to DNP-decorated DON. (A) Schematic illustration of DNP-decorated DON arrangements designed for monovalent (four DNP ligands, top) and bivalent (eight DNP ligands, shown here for the two designs B<sub>6</sub> and B<sub>30</sub>, bottom) binding. The designs of all DNP-decorated DON reagents used are shown in Figure S2. The representative AFM image was obtained from the DNP–DON B<sub>16</sub> incubated with 3 eq of anti-DNP IgG. Scale bar: 50 nm. (B) Schematic illustration showing that antibodies, depending on their segmental Fab flexibility, can bind in a mono- or bivalent fashion to DNP ligands arranged on the DON at varying distances (6–30 nm). (C) SPR sensorgrams of single cycle kinetics with anti-DNP IgE. Averaged data of triplicates is shown. (D) Dissociation rate  $k_d$  of anti-DNP IgE, derived from SPR sensorgrams by fitting the data of the 0–1500 s increment from (C) to a 1:1 Langmuir binding model. (E) SPR sensorgrams of single cycle kinetics with anti-DNP IgG. Averaged data of triplicates is shown. (F) Dissociation rate  $k_d$  of anti-DNP IgG, derived from SPR sensorgrams by fitting the data of the 0–1500 s increment from (E) to a 1:1 Langmuir binding model. Error bars in (D) and (F) indicate the standard deviation from three independent experiments.

**Spatial Arrangement of DNP Ligands Affects Bivalent Binding of Antibodies.** The following goal was to investigate the specific antibody–hapten binding. Here, the spatial tolerance for bivalent binding of the antibody–Fabs with different distances between the hapten ligands was of special interest. To achieve this, we designed DNP-decorated DON containing four single DNP ligands per DON for monovalent binding (design M, Figure 2A) as well as a set of DON that contained four DNP–ligand pairs (eight DNP ligands) arranged with variable spacing from 6 to 30 nm (designs

B<sub>6</sub>–B<sub>30</sub>, Figure 2A,B). For details of the designs, see Figure S2. To investigate the interaction of IgE antibodies with the varying DON designs, we measured binding kinetics using the label-free surface plasmon resonance (SPR) spectroscopy technique. This was achieved by immobilizing the DON in a BIAcore X-100 instrument (Cytiva) via DNA hybridization over the protruding staple strands and quantifying the binding of IgE in real time. Specifically, for DON immobilization, we functionalized a high-affinity streptavidin (SA) sensor chip with biotinylated capture oligonucleotides, whose sequence is

complementary to the protruding oligonucleotides of DON. DNP-decorated DON were immobilized on the active flow cell (Fc2), and a reference DON without DNP modification was immobilized on the reference flow cell (Fc1) for control and background subtraction (Figure S3). After DON immobilization, the binding of antibodies to the hapten-decorated DON was measured in real time, as previously described by Högberg and colleagues.<sup>37</sup>

We performed single-cycle kinetics where the analyte (IgE) was sequentially injected in five different concentrations and without regeneration between sample injections. To this end, serial dilutions of anti-DNP IgE (1.25–20 nM) were injected with a subsequent dissociation phase of 20 min (Figure 2C,D). Similar measurements were also performed with an anti-DNP immunoglobulin G (IgG, 31.25–500 pM) to elucidate specific differences in the binding behavior of these two important antibody classes, which are both involved in the immediate immune response in mast cell regulation (Figure 2E,F). For kinetic analysis, the 0–1500 s increment of the obtained SPR sensorgrams were fitted to a 1:1 Langmuir binding model (Figure S4) to minimize the effect of complex secondary binding events such as rebinding and “walking” of antibodies.<sup>38</sup> To facilitate a qualitative comparison of the kinetic data, the same fitting model was applied to the entirety of the samples to identify differences in the dissociation rate  $k_d$  (Figure 2D,F and Tables S1 and S2) and immune complex half-life time  $t_{1/2}$  (Figure S5) of the antibody–DON complex. It should be noted that although the dissociation rate of the 1:1 Langmuir binding model does not provide kinetic information about bivalent binding, it does provide accurate data regarding the stability of the complex formed, which correlates with the spatial tolerance for bivalent binding of the antibodies.

Kinetic data obtained by SPR spectroscopy showed a pronounced distance dependence for bivalent binding of the two antibody classes. DON with four DNP ligands were used as monovalent samples, arranged in such a way that only monovalent binding (distance >37 nm) of an antibody Fab fragment should be possible. By using the three different designs ( $M_a$ ,  $M_b$ ,  $M_c$ , see Figure S2), which differ slightly from each other in the positioning of the four DNP ligands, we wanted to first test the reproducibility of the method in terms of ligand positioning on the DON. For this purpose, the four DNP ligands were arranged with varying positions inside and also at the edges of the DON. In doing so, the widest possible spacing could be created in an attempt to prevent a bivalent bridging of antibodies across multiple DNP ligands. Indeed, as indicated by the sensorgrams and dissociation rates, all monovalent samples showed almost identical low response values and fast dissociation rates (Figure 2C–F), especially when compared to samples where a bivalent binding was observed (Tables S1, S2).

In contrast, an approximately 3-fold increase in the overall response was observed when four DNP pairs instead of four single DNP ligands were placed on the DON (designs B\_6–B\_30). These SPR data indicate additional binding events and thus mass accumulation on the sensor surfaces (Figure 2C–F, Tables S1 and S2). The sensorgram curvature and dissociation rates for the samples with large distances (24–30 nm) were similar to those of the monovalent samples (i.e.,  $k_d$  ( $M_c$ ) =  $6.2 \times 10^{-3} \text{ s}^{-1}$ ,  $k_d$  (B\_30) =  $6.8 \times 10^{-3} \text{ s}^{-1}$  for anti-DNP IgE and  $k_d$  ( $M_c$ ) =  $2.2 \times 10^{-3} \text{ s}^{-1}$ ,  $k_d$  (B\_30) =  $2.0 \times 10^{-3} \text{ s}^{-1}$  for anti-DNP IgG). Lower dissociation rates and thus higher complex half-lives ( $t_{1/2} = \ln(2)/k_d$ ) were observed at distances between

12–18 nm and 6–18 nm for anti-DNP IgE and anti-DNP IgG, respectively, suggesting a suitable DNP spacing range for bivalent binding of the antibodies. Spacing the DNP ligands at distances outside of this range seemed to weaken or prevent strong bivalent binding of the antibodies to the DNP-decorated DON. The data obtained from the dissociation constants and complex half-lives also showed that the overall binding strength of anti-DNP IgG to the DNP-decorated DON was approximately 10-fold higher than that of the anti-DNP IgE antibody (Figure S5). The highest binding stability was observed at a DNP distance of 16 nm for anti-DNP IgE ( $k_d = 2.6 \times 10^{-3} \text{ s}^{-1}$  and  $t_{1/2} = 4.5 \text{ min}$ ) and 6–18 nm for anti-DNP-IgG (e.g.,  $k_d = 2.1 \times 10^{-4} \text{ s}^{-1}$  and  $t_{1/2} = 68 \text{ min}$ , for DON B\_16). Consequently, IgG showed greater segmental flexibility than IgE, as indicated by the wider U-shape when comparing the plot of  $k_d$  versus DNP distance on the DON (Figures 2D,F).

Compared to IgG, the anti-DNP IgE antibody exhibited a narrower window for bivalent binding. These results are consistent with structural data showing that, in contrast to IgE, the Fc and Fab fragments of IgG are linked by a flexible amino acid segment in the hinge region. This allows segmental flexibility and thus a broader binding range for antigens.<sup>39</sup> The Fab–Fab distance of different IgG subclasses ranges between 11 and 16 nm as determined by X-ray crystallography.<sup>40</sup> However, segmental flexibility had been previously observed using cryo-electron microscopy where the Fab positions of IgG antibodies in solution showed great variation.<sup>41</sup> In addition, bivalent binding at small Fab–Fab distances was reported for IgG antibodies in complex with human rhinovirus serotype 2 (HRV2) whose symmetrical epitopes are distanced only 6 nm apart from each other.<sup>42</sup> While several crystallographic studies investigated the structure of the crystallizable fragment (Fc) of IgE,<sup>43–45</sup> information on the Fab fragments and the intact structure of IgE under physiological conditions could only be derived from a recent study as of yet. This was based on small-angle X-ray scattering and negative stain electron microscopy.<sup>46</sup> Here, a native Fab–Fab distance of IgE of  $\sim 15 \text{ nm}$  was found which turned out to be in good agreement with our own finding that IgE forms the strongest bivalent bond at a ligand distance of 16 nm.

Since both IgG and IgE antibodies are elicited against immunogenic determinants during the immune response, their affinity for antigens and, in the case of IgE, for the FcεRI receptor plays an important role in physiological processes. The differences observed here in the total binding strength and spatial tolerance for bivalent binding of IgE and IgG may therefore be related to their different roles in immune responses. Concentrations of IgE in the bloodstream are about 100-fold lower compared to IgG concentrations (100 ng/mL versus 10 mg/mL). This correlates with the high-affinity binding of IgE to the FcεRI receptor and the fact that mast cells express several receptors with low affinity for IgG.<sup>47</sup> Furthermore, in mast cell signaling, allergen-specific IgG antibodies can inhibit IgE-mediated degranulation either through competitive binding to IgE-binding epitopes or receptor-mediated inhibition through allergen-mediated cross-linking of IgE–FcεRI with IgG–FcγRIIb.<sup>47</sup> Thus, there is a balance between IgG and IgE antibody binding that modulates the immunoregulatory effects of mast cells. The results presented here offer a quantitative approach describing the interactions between antibodies and mast cells in detail and

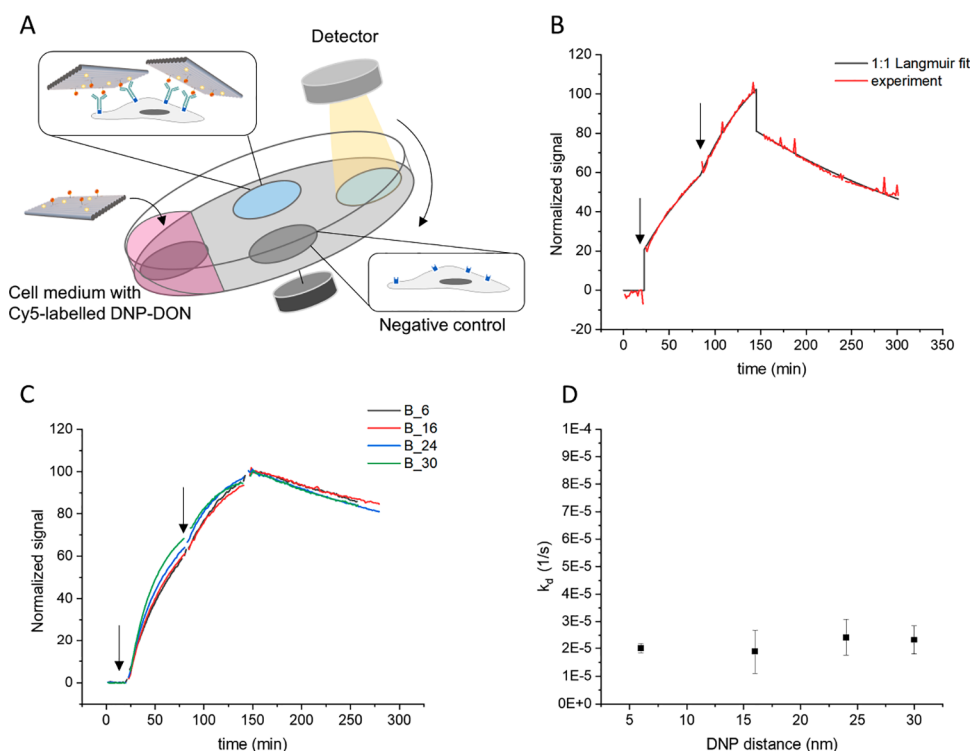


**Figure 3.** Binding studies of receptor-bound anti-DNP IgE against DNP-decorated DON. DON designs are similar to those used in SPR analyses (see Figure S1). (A) Schematic illustration of experimental Ligand Tracer setup. RBL-2H3 cells were cultivated on a four-well Petri dish and incubated in medium containing (blue area) or lacking (gray area) anti-DNP IgE. Cy5-labeled DNP–DON was introduced into the medium as the analyte and the dish was placed on an inclined rotating support. A detector measured the change in fluorescence intensity in the target and control regions during rotation. (B) Ligand Tracer sensorgram of Cy-5 labeled anti-DNP IgE binding to RBL-2H3 cells. Binding was measured at concentrations of 2.5 and 5 nM (as indicated by arrows). The sensorgram was fitted using a 1:1 Langmuir binding model. (C) Ligand Tracer sensorgrams of Cy5-labeled DNP–DON binding to RBL-2H3 cells sensitized with anti-DNP IgE. Binding was measured at concentrations of 0.8 nM and 1.6 nM (as indicated by arrows). Averaged data of triplicates is shown. (D) Dissociation rate  $k_d$  (1/s) derived from Ligand Tracer sensorgrams by fitting the data from (C) to a 1:1 Langmuir model.

should thus contribute to a better understanding of the overall processes.

**Spacing of DNP Ligands Does Not Affect Binding Affinity of Receptor-Bound IgE.** To further explore the effects of nanoscale DNP spacing in a biological context, we wanted to test whether our results on spatial tolerance for strong bivalent binding of free IgE antibodies correlate with those of receptor-bound IgEs. For this purpose, we used the RBL-2H3 cell line, which is an established model cell line for mast cells.<sup>11</sup> However, as it is an adherent cell line, the experimental SPR setup with RBL-2H3 cells as the analyte is not feasible due to the high background binding of the cells to the sensor chip surface (data not shown). Therefore, we used a different approach, namely Ligand Tracer technology (Figure 3A),<sup>48</sup> to measure the interaction between cellular receptor and antibody or DNP–DON on living cells in real-time. For this approach, RBL-2H3 cells were first seeded and cultured overnight on a fibronectin-coated four-well Petri dish to obtain a confluent monolayer of cells. Other cells or reagents that interact with the RBL-2H3 cells can be placed in the four wells. Since the walls of these wells are flat, they can be washed over by a volume of liquid medium when the dish is incubated in a tilted rotating manner (Figure 3A). Thus, independent binding experiments with a Cy5-labeled analyte in the medium can be performed simultaneously, including the positive and negative control. In a typical experiment, the binding of the Cy5-labeled analyte to the cells in the first stage is monitored by measuring the fluorescence increase of the cell patches in the wells with a

detector. In the second phase, the medium is exchanged and the dissociation of the analyte can be measured by the decrease in fluorescence. Subtraction of the fluorescence values from the negative controls then leads to sensorgrams that can be fitted to a Langmuir binding model, for example, and provide kinetic data.

In a first set of experiments, we investigated the antibody–receptor interaction of anti-DNP IgE to the FcεRI on living cells. Here, Cy5-labeled anti-DNP IgE was added to the medium in two different concentrations (2.5 and 5 nM) and incubated in the rotating dish. For the negative control either a random cell line (MDA-MB-231), which does not express the target receptor FcεRI, or simply no cells were used. This allowed the signal correction of unspecific binding of the Cy5-labeled analyte to the cell surface or the Petri dish (Figure S6). The obtained sensorgrams were fitted to a 1:1 Langmuir binding model for kinetic analysis using TraceDrawer software (Ridgeview Instruments AB) (Figure 3B). In this case, we calculated that the equilibrium constant  $K_D$  as the binding of the IgE–Fc to FcεRI is a real 1:1 interaction. We found strong binding with a dissociation equilibrium constant  $K_D = 1.3 \times 10^{-9} \text{ M} \pm 3.6 \times 10^{-10} \text{ M}$ , consistent with affinities reported in the literature for this interaction ( $K_D = 10^{-9}–10^{-10} \text{ M}$ ).<sup>49,50</sup>

Next, we wanted to investigate the spatial tolerance of anti-DNP IgE antibodies bound to the cell surface to FcεRI. For this purpose, we used RBL-2H3 cells that were initially incubated with anti-DNP IgE. The same cell line missing antibody sensitization was used as a negative control (see

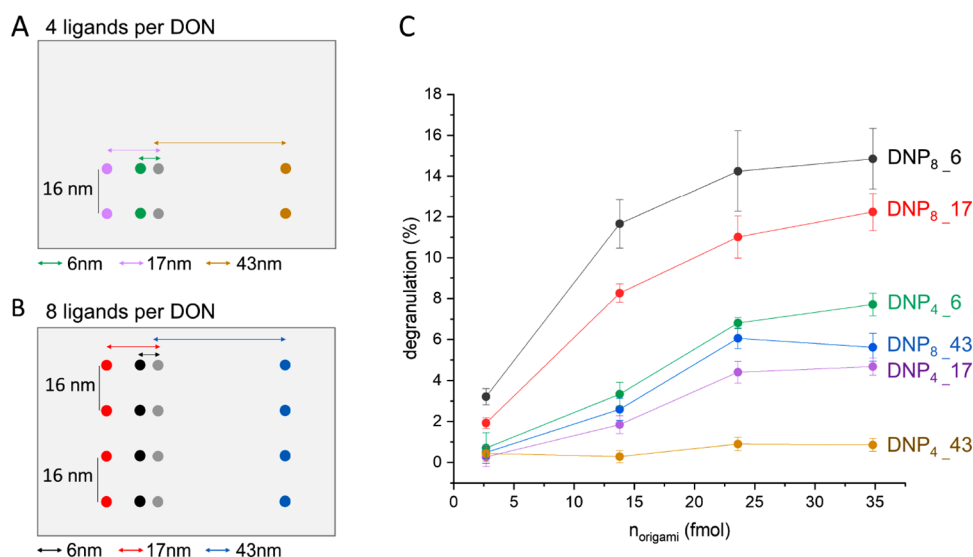


**Figure 4.** Investigation of the cell activation of RBL-2H3 cells. Cells were introduced to surface-immobilized DNP–DON constructs with varying ligand stoichiometries and arrangements. (A) Schematic illustration of DNP–DON constructs bearing four DNP ligands per DON, as represented by two gray and two different colored dots each. The constructs were designed to induce antibody arrangements with intermolecular distances of 6, 17, or 43 nm in the cell membrane, as indicated by the colored arrows. (B) Schematics of DNP–DON containing eight DNP ligands with distances of 6–43 nm, indicated analogously to (A). It should be noted that the spacing between DNP rows of 16 nm is to facilitate the binding of one IgE per two and four antibody molecules per DON, which can serve as a starting point for supramolecular receptor clustering. (C) Degranulation of anti-DNP IgE-sensitized RBL-2H3 cells after incubation on immobilized DNP–DON containing four or eight DNP ligands in the different arrangements shown in A and B. The data shows the result of a representative experiment ( $n = 3$ ), and the error bars show the typical standard deviation of technical triplicates. Note that additional negative and positive control groups were examined with degranulation assays using reference DON lacking DNP ligands for the former and surface-bound DNP ligands not arranged on DON for the latter (Figure S11, see also Figure S8).

Figure 3A) to distinguish nonspecific adsorption from specific binding of Cy-5-labeled DNP–DON. Binding curves were measured for selected DNP–DON samples with variable DNP distances ranging from 6–30 nm, each of which was used at two different concentrations (0.8 and 1.6 nM) in the binding phase before the medium was exchanged in order to determine the analyte dissociation (Figure 3C). Surprisingly, we observed that the overall shape of the sensorgrams was almost identical for all samples and resulted in very similar dissociation rates that were almost independent of the spacing of the DNP ligands on the DNP–DON (Figure 3C,D). This suggested that the spatial arrangement of the ligands did not affect the binding strength of the receptor-bound IgE antibodies ( $k_d = 1.9\text{--}2.4 \times 10^{-5} \text{ s}^{-1}$ , see Table S3). Considering the dissociation rate determined for the (more stable) bivalent binding of free IgE ( $k_d = 2.6 \times 10^{-3} \text{ s}^{-1}$  for B<sub>16</sub>, Table S1), the approximately 100-fold slower dissociation rate measured for receptor-bound IgE ( $k_d = 1.9 \times 10^{-5} \text{ s}^{-1}$  for B<sub>16</sub>, Table S3) suggests that incorporation of the antibodies into the Fc $\epsilon$ RI–IgE complex in the cell membrane leads to a more stable interaction with the antigen. This hints at an oligovalent nature of the binding.

Consistent with the hypothesis of an oligovalent interaction, the lack of distance dependence in the previous experiment may be due to the fact that IgE–Fc $\epsilon$ RI complexes are free to diffuse in the cell membrane. Binding of these complexes with antigens can induce the formation of macromolecular cluster assemblies that exhibit restricted lateral mobility.<sup>51</sup> The formation of cluster assemblies leads to a very high local concentration of receptor-bound IgE antibodies and thus Fab fragments, each of which can then bind monovalently to the antigen. In doing so, they can still lead to a supramolecular

oligovalent type of interaction with high overall stability of receptor-antigen binding that may even exceed simple bivalent binding. The transition from rather weak monovalent ligand-protein interaction to stable “superselective” multivalent ligand binding can occur when the receptors have lateral mobility in the cell membrane, as recently emphasized by Bastings and colleagues,<sup>36,52</sup> which can also be exploited for diagnostic purposes.<sup>53</sup> This consideration, based on quantitative data, led us to hypothesize that spatial tolerance for bivalent binding of receptor-bound IgE antibodies does not play a decisive role in affinity toward the antigen. This is because it may be that supramolecular oligovalency is the dominant binding mode in antibody–receptor cluster assemblies.

**Mast Cell Degranulation Can Be Modulated with Nanoscaled DNP Arrays.** Since it is well-known that antigen-mediated spatial organization of IgE–Fc $\epsilon$ RI complexes into cluster assemblies can initiate the release of inflammatory mediators,<sup>54</sup> we wanted to further substantiate the working hypothesis above. This was attempted by using specifically designed DNP–DON in order to influence the assembly of Fc $\epsilon$ RI-bound IgE–hapten complexes and thus the cellular response. To measure the cell activation triggered by DNP–DON, the secretion of  $\beta$ -hexosaminidase from the cell granules into the supernatant was quantified by enzymatic cleavage of the fluorogenic substrate 4-methylumbelliferyl-*N*-acetyl- $\beta$ -D-glucosaminide (MUG).<sup>55</sup> To perform this assay, we immobilized DNP–DON on the surface of 96-well microtiter plates via their protruding capture oligonucleotides by specific DNA hybridization. The amount of surface-immobilized DON was determined by quantitative PCR (qPCR) (Figure S7). Subsequently to DON immobilization and the washing of the wells to remove unbound DON, cells were added to the

wells and incubated for 1 h. The supernatant containing the degranulated  $\beta$ -hexosaminidase was mixed with the MUG substrate solution, and the enzymatic reaction was stopped after 30 min by adding glycine carbonate buffer at pH 10. Cell activation was quantified by the fluorescence of the cleaved substrate and normalized to the maximum  $\beta$ -hexosaminidase activity determined in the lysate after cell solubilization with 0.1% Triton X-100.

First, we tested several of the previously characterized DNP–DON designs used for the binding analysis of IgE to DON, i.e., the DNP arrays originally developed to study the spatial tolerance of antibodies to bivalent binding. These carried four DNP pairs with varying interligand distances on the DON to test the intramolecular binding distance of Fab fragments (B<sub>6</sub>–B<sub>30</sub>). Details are given in Figure S8. However, we found only a low secretion of  $\beta$ -hexosaminidase, despite the fact that we tested different concentrations and even added cytochalasin D to the medium, which acts as an inhibitor of actin polymerization and is known to enhance Fc $\epsilon$ RI-mediated degranulation.<sup>56,57</sup> We attributed these results to the occurrence of the supramolecular oligovalent interactions discussed above, which could possibly result in high overall stability of receptor–antigen binding and thus cell activation independent of high-affinity nanostructured arrangements of the ligands.

In light of the previously outlined results of the study of Fc $\epsilon$ RI-bound IgE (Figure 3), we then designed new DNP–DON constructs to promote receptor clustering using DNP arrays with different intermolecular spacing. This was meant to lead to increased receptor clustering and, thus, cell activation and degranulation. Inspired by work showing that both intramolecular ligand spacing for binding a multivalent binding partner and intermolecular spacing between binding partners can contribute to a maximal signal response,<sup>52</sup> we arranged DNP ligands in two columns. Here, we designed the DNP–DON constructs with two different stoichiometries (four or eight DNP per DON) and placed the two columns at different distances to one another (6, 17, and 43 nm). Specifically, the distance between DNP rows was chosen as 16 nm in order to enable tight binding of one IgE per two DNP ligands, thus fixing two and four antibody molecules per DON, acting as an initiation point for supramolecular receptor clustering. The designs used are shown schematically in Figures 4A,B, and details of the DON structure are given in Figures S9 and S10. The DNP positions on the DON were verified by AFM (Figure S10). A reference DON, which did not contain DNP ligands, was used as a negative control for the cell assay, whereas the entire surface of the well was saturated with biotinylated DNP ligands for the positive control causing a maximum surface density of DNP to be present (Figure S11).

The results of the cell degranulation studies are shown in Figure 4C. First, it should be noted that a distinct trend in concentration-dependent degranulation was observed, as was to be expected. More ligand leads to stronger degranulation. This is clearly evident when comparing DNP–DON that have the same intermolecular spacing of ligands yet different valency, such as DNP<sub>4</sub>\_17 (magenta curve in Figure 4C) and DNP<sub>8</sub>\_17 (red curve), which bear four and eight DNP ligands, respectively. Likewise, higher cell activation was also observed for the other samples with higher valency. This finding is not surprising, as it has been previously shown that antigen valency is a crucial factor for efficient and robust cross-

linking of IgE–Fc $\epsilon$ RI complexes, even in cases with low-affinity allergens.<sup>58</sup>

A particularly interesting finding, however, was the fact that there was a distinct trend in distance-dependent cell degranulation that occurred based on the variable intermolecular distances of our DNP–DON with DNP<sub>8</sub>\_6 nm > DNP<sub>8</sub>\_17 nm > DNP<sub>8</sub>\_43 nm or DNP<sub>4</sub>\_6 nm > DNP<sub>4</sub>\_17 nm > DNP<sub>4</sub>\_43 nm. In fact, the nanoscale spacing effect can even be observed exceeding the valency effect, as is evident when comparing DNP<sub>4</sub>\_17 with DNP<sub>8</sub>\_43. Here, two ligands with 17 nm spacing have a stronger activation power than four ligands with 43 nm spacing. In summary, these experiments demonstrate that the effect of ligand patterns and spacing may be more crucial for cell activation compared to the sheer number of ligands. In addition, the results allow conclusions to be drawn about the influence of nanoscale antigen architecture on the formation of receptor clusters. In this respect, our results show that a larger distance seems to hinder the effective formation of receptor clusters. This is exemplified by DNP<sub>4</sub>\_43, where robust cell degranulation could not be observed for any amount of immobilized DON (<1% degranulation for any amount of immobilized DNP–DON). Through Ligand Tracer experiments, we were also able to confirm that the pronounced differences in cell degranulation did not correlate with the binding parameters of Fc $\epsilon$ RI-bound IgE to the different DNP arrays on the DON samples (Figure S12, Table S4). For example, DNP<sub>4</sub>\_6 had a slightly lower interaction strength with the sensitized cells than DNP<sub>4</sub>\_17 and DNP<sub>4</sub>\_43. Therefore, the results demonstrate an apparent spatial factor that influences the cell activation. This is presumably amplified by downstream phosphorylation of immune receptor tyrosine-based activation motifs (ITAMs) that leads to degranulation.<sup>6,7</sup>

Overall, it can be concluded that the DNP–DON approach allows control over the location and size of receptor clusters not only by means of valency but also by modification of the spatial organization of IgE–Fc $\epsilon$ RI complexes. In this approach, Fc $\epsilon$ RI cross-linking is achieved by using a multivalent antigen with precise nanoscale ligand arrangement that is then presented on a surface rather than as a soluble stimulus. Surface-based presentation of nanopatterned ligands is of particular interest when studying interactions at cell–cell contact sites or receptor ligands in the extracellular matrix.<sup>59</sup> Therefore, other surface-based methods using supported lipid bilayers with hapten-labeled lipids have been used to demonstrate localized stimulation, yet only at micron-scale lateral resolution.<sup>60–63</sup> Our approach offers clear advantages here, as spatial control is achievable at both the micrometer and nanometer scales. In addition, the multivalent ligand presentation on a rigid surface used herein may be better suited to study antigens that are arranged in a rigid lattice. This is the case for several human or animal pathogens whose surfaces can be considered quasi-crystalline.<sup>64</sup>

## SUMMARY AND CONCLUSIONS

In the present study, we report on 2,4-dinitrophenyl (DNP)-decorated DNA origami nanostructures for the structural investigation of the spatial tolerance of antibody Fabs for bivalent binding, binding kinetics of free and receptor-bound antibodies and, finally, nanopatterned controlled degranulation of a model cell line for mast cells. In SPR spectroscopy studies, anti-DNP IgG showed a more pronounced spatial tolerance and a 10-fold stronger binding to DNP-ligands presented on

the DON surface when compared to anti-DNP IgE. Increased complex stability at binding ranges between 6–18 nm for anti-DNP IgG and 12–18 nm for anti-DNP IgE was observed, suggesting a bivalent binding mode at these distances.

Real-time interaction measurements of DNP–DON with Fc $\epsilon$ RI-bound IgEs on the surface of living RBL-2H3 cells revealed no nanoarchitectural influences in the binding of DNP–DON with different DNP distances to cellular antibodies. This is presumably due to the lateral mobility of Fc $\epsilon$ RI–IgE complexes in the cell membrane,<sup>61</sup> which leads to a supramolecular oligovalency-like interaction in the formation of antibody-receptor cluster assemblies. To further elucidate cell activation, we then presented the hapten-decorated DON on solid surfaces to provide a stimulatory interface for antibody-mediated receptor interaction. Here, we found that degranulation was regulated in a concentration- and distance-dependent manner by hapten arrangements on the DON, where higher degranulation was found at small distances (6 nm < 17 nm < 43 nm). Since our approach allows us to present the exact number and position of ligands on defined nanostructures, we were able to show that the same spacing effect also occurs for constructs with higher valency, while, at the same time, the intensity was varied (DNP<sub>8\_x</sub> > DNP<sub>4\_x</sub>). In fact, we could even show that the nanoscale spacing in the ligand arrays seems to be more crucial for cell degranulation than the total number of ligands.

In summary, this work demonstrates how concepts of DNA nanotechnology can be used to achieve control over valency and nanoscale spacing of hapten molecules for studying biological processes. However, the insights gained in respect to antibody dynamics under physiological conditions, as well as in the initial binding events involved in mast cell effector function, should only be considered as one example of the power of the method. This experimental setup can easily be transferred to clinically relevant systems by immobilizing naturally occurring allergens, such as pollen allergens,<sup>58,65</sup> onto DON via appropriate protein bioconjugation methods,<sup>66</sup> instead of small molecules. For instance, this could allow the study of inflammatory responses in type I allergies, such as passive cutaneous anaphylaxis.<sup>61</sup> However, since the DNP-decorated DON showed no deleterious effects on cells in cytotoxicity assays (Figure S13), constructs of this type could also potentially be used as a soluble stimulus. This would allow the application of hapten-decorated DON *in vivo*, as has been suggested for other immunostimulatory DNA nanostructures.<sup>67</sup> Moreover, since DNA origami can also be immobilized on nanoparticles and microparticles,<sup>68</sup> the development of particulate formulations with surface-bound hapten–DON constructs for immunostimulation also appears feasible. We believe that this proof-of-principle study provides a solid basis for further studies that may be conducted to elucidate fundamental molecular mechanisms of binding events that occur in immunology and numerous other biological processes.

## EXPERIMENTAL SECTION

**Design of DNA Origami Nanostructures.** Rectangular DNA origami nanostructures (DON) were designed using the single-stranded scaffold p7560 (Tilbit nanosystems) and 240 staple-strand oligonucleotides (Sigma-Aldrich) as described previously.<sup>53</sup> Several staple strand oligonucleotides were modified at the 5' end to incorporate Cy5 fluorophores and 2,4-dinitrophenol (DNP) ligands on the upper side of the DON and protruding single-stranded oligonucleotides 24 bases long on the lower side of the DNA origami for immobilization of the DON via hybridization. Lower and upper

side refer to the position on the DON plane after binding on a surface. Sequences are listed in Tables S5–S7, and modified positions on the DON are illustrated in Figure S1.

### Assembly and Purification of DNA Origami Nanostructures.

For DON assembly, staple oligonucleotides were used in a 10-fold molar excess to the single-stranded scaffold p7560 (20 nM) in TE-Mg<sub>15</sub> mM buffer (20 mM Tris base, 1 mM EDTA, 15 mM MgCl<sub>2</sub>, pH 8.0). Self-assembly reaction was conducted in a Thermocycler (Eppendorf Master cycler pro), with an initial denaturation step for 5 min at 95 °C and a subsequent stepwise temperature decrease from 75 to 25 °C with a cooling rate of –0.1 °C/s. To purify the DON after annealing, the excess of staple strands was removed by PEG-precipitation according to Dietz's procedure<sup>69</sup> by adding precipitating buffer (5 mM Tris base, 1 mM EDTA, 505 mM NaCl, 15% PEG-8000) in a 1:1 volume ratio and subsequent centrifugation (16100 g, 30 min, 20 °C). The obtained DON pellet was washed and resuspended in 50  $\mu$ L TE-Mg<sub>6</sub> mM buffer (20 mM Tris base, 1 mM EDTA, 6 mM MgCl<sub>2</sub>, pH 7.6) for storage at 4 °C.

**Quantitative Polymerase Chain Reaction.** Quantitative polymerase chain reaction (qPCR) was used to determine DON concentration based on a calibration curve of the single-stranded scaffold p7560 in the range of 15 nM to 150 fM in triplicates. For the preparation of 10 mL of qPCR Master Mix, 1 mL of 10 $\times$  qPCR Buffer (160 mM (NH<sub>4</sub>)<sub>2</sub>SO<sub>4</sub>, 670 mM Tris-HCl, 25 mM KCl, and 25 mM MgCl<sub>2</sub>, 0.1% v/v Tween 20), 200  $\mu$ L dNTPs (10 mM each), 100  $\mu$ L of forward primer (100  $\mu$ M, CCAACGTGACCTATCCCATTAC), 100  $\mu$ L of reverse primer (100  $\mu$ M, TTCCTGTAGCCAGCTTT-CATC), 20  $\mu$ L of TaqMan3 probe (100  $\mu$ M, FAM-CGACGGGTTGTTACTCGCTCATAT-TAMRA), and 100  $\mu$ L of Taq DNA Polymerase (5 U/ $\mu$ L) (New England Biolabs) were combined in autoclaved H<sub>2</sub>O. For the qPCR, 20  $\mu$ L of qPCR Master Mix was mixed with 1.5  $\mu$ L of p7560 calibration standards or DON samples, and measurements were conducted using a real-time thermocycler (Corbett research). The cycle threshold (Ct) signal was subtracted from the maximum number of cycles (C<sub>Max</sub>) and  $\Delta$ Ct values were plotted against the log concentration of the p7560 calibration in order to receive DON concentrations by means of linear regression.

**Atomic Force Microscopy.** For DON characterization via atomic force microscopy (AFM), 112.5 fmol of DON sample was incubated with a 3-fold molar excess of anti-DNP IgG in regard to DNP-binding sites present on the DON for 30 min at room temperature. Afterward, the reaction mixture was diluted to a final concentration of 3 nM DON using TeMg<sub>12.5</sub> mM buffer (20 mM Tris base, 1 mM EDTA, 12.5 mM MgCl<sub>2</sub>, pH 7.6) and 5  $\mu$ L was added on a freshly cleaved mica disc (Plano GmbH) for 3 min at room temperature. Afterward, 10  $\mu$ L of TeMg<sub>12.5</sub> mM buffer was added on top and DON were imaged in liquid using SNL-10 cantilevers ( $k = 0.35$  N m<sup>-1</sup>,  $r = 2$  nm, Bruker) and tapping mode on a MultiModeTM 8 atomic force microscope (Bruker) equipped with a NanoScope V controller. The obtained images were analyzed using the NanoScope Analysis software (Bruker).

**Surface Plasmon Resonance Spectroscopy.** For Surface Plasmon Resonance (SPR) spectroscopy, we used a BIAcore X-100 instrument (Cytiva) with a SA sensor chip (Cytiva) containing immobilized streptavidin in a dextran matrix for high-affinity binding of biotinylated ligands. To capture the DNP-decorated-DON on the surface, we first immobilized biotinylated capture oligonucleotides with the complementary sequence to the protruding oligonucleotides of the DON. Through hybridization, the DNP-decorated DON were immobilized on the active flow cell (Fc2) and a reference DON without any DNP ligands was immobilized on the reference flow cell (Fc1). This was done to correct the active signal for unspecific binding of the anti-DNP antibody to the surface of the sensor chip or DON (Fc2–Fc1). Biotinylated capture oligonucleotides (200 nM) were injected in HBS-EP running buffer (0.01 M HEPES, 0.15 M NaCl, 3 mM EDTA, 0.005% v/v Tween 20, pH 7.4) over the surface of both flow cells with a flow rate of 10  $\mu$ L/min for 3 min. Subsequently, three short injections (60 s) of 50 mM NaOH removed any nonspecifically bound oligonucleotides. The DNP-decorated

DON ( $c = 160\text{--}200$  nM) were injected with a flow rate of  $5\ \mu\text{L}/\text{min}$  until an immobilization level of 400 response units (RU) was reached ( $\sim 30$  min). Two (anti-DNP IgG) or three (anti-DNP IgE) startup-cycles with bovine serum albumin (BSA,  $2\ \text{mg}/\text{mL}$  in running buffer,  $30\ \mu\text{L}/\text{min}$ , 5 injections) were performed to reduce any unspecific binding of the antibody to the surface. For single cycle kinetics, anti-DNP IgE or anti-DNP IgG was injected in five different concentrations (IgE:  $1.25$  nM,  $2.5$  nM,  $5$  nM,  $10$  nM,  $20$  nM, IgG:  $31.25$  pM,  $62.5$  pM,  $125$  pM,  $250$  pM,  $500$  pM), starting from the lowest concentration to the highest, during a contact time of  $120$  s. A flow rate of  $30\ \mu\text{L}/\text{min}$  was used to avoid mass transfer limitations. After injection of the highest concentration, the dissociation of the antibody from the surface was recorded for  $20$  min. To regenerate the surface for the next experiment,  $50$  mM NaOH ( $10\ \mu\text{L}/\text{min}$ ,  $120$  s) was injected after every single cycle. The kinetic evaluation was performed using the BIAcore x100 Evaluation Software (Cytiva). Sensorgrams were background corrected by subtraction of a sensorgram with EBS-HP running buffer without analyte, which was performed before every single cycle. The sensorgrams were fitted to a 1:1 Langmuir binding model between  $0\text{--}1500$  s with bulk refractive index contribution (RI) set to  $0$ . Monoclonal mouse anti-DNP IgE (clone SPE-7) was purchased from Sigma-Aldrich, and monoclonal rat anti-DNP IgG (clone LO-DNP-2) was purchased from Thermo Fisher Scientific.

**Cell Culture.** All medium components and reagents used in cell culture were purchased from Gibco Life Technology if not stated otherwise.

**RBL-2H3 Cells.** Adherent RBL-2H3 cells, kindly provided by Prof. Andrew Cato (KIT), were cultured in RBL-2H3 culture medium (70% RPMI-1640, 20% MEM  $\alpha$  medium, 10% fetal bovine serum (Sigma-Aldrich) supplemented with  $100$  U/mL of penicillin, and  $100\ \mu\text{g}/\text{mL}$  streptomycin (Thermo Fisher)). For passaging, cells at 90% confluency were washed with  $10$  mL of  $1\times$  PBS buffer (Gibco), harvested by treatment with TrypLE for  $5$  min ( $37\ ^\circ\text{C}$ ,  $5\%$   $\text{CO}_2$ ), and seeded in Nunc EasY Flasks ( $75\ \text{cm}^2$ , Thermo Scientific) with a final volume of  $15$  mL and a cell seeding density of  $0.1 \times 10^6$  cells/mL. Cells were incubated in a cell incubator (Binder) with a  $\text{CO}_2$  atmosphere of  $5\%$  at  $37\ ^\circ\text{C}$  and passaged every  $3\text{--}4$  days. For cell experiments, cells were harvested, then counted using a hemocytometer (Marienfeld Superior), and centrifuged at  $1300g$  for  $5$  min at room temperature. Subsequently, the cell pellet was resuspended in RBL-2H3 culture medium or buffer to yield the desired cell density.

**MDA-MB-231 Cells.** Human MDA-MB-231 breast cancer cells were kindly provided by Prof. Ada Cavalcanti (MPI for Medical Research, Heidelberg) and cultured in high glucose DMEM medium supplemented with  $1\%$  GlutaMAX,  $1\%$  Pen/Strep and  $10\%$  fetal bovine serum (Sigma-Aldrich). Cells were grown at  $37\ ^\circ\text{C}$  in a humidified atmosphere with  $5\%$   $\text{CO}_2$  and harvested at  $90\%$  confluency.

**Determination of Cell Viability.** Cell viability of RBL-2H3 cells was determined by a colorimetric assay using 3-(4,5-Dimethylthiazol-2-yl)-2,5-diphenyltetrazolium bromide (MTT), as described elsewhere.<sup>70</sup> RBL-2H3 cells were harvested at  $90\%$  confluency and sensitized with anti-DNP IgE ( $1\ \mu\text{g}/\text{mL}$ ) for  $1$  h at  $37\ ^\circ\text{C}$ . Cells were washed with PBS buffer, resuspended in RBL-2H3 cell culture medium, and seeded in the wells of a 96-well plate ( $4000$  cells/well).  $50\ \mu\text{L}$  of DNP-DON samples were added at various concentrations ( $c_{\text{final}} = 0.02, 0.1, 0.4, 1$  nM), and cells were incubated at  $37\ ^\circ\text{C}$  in a humidified atmosphere with  $5\%$   $\text{CO}_2$  for  $24$  h. Subsequently, the supernatant was discarded, and a solution of DMEM medium supplemented with MTT ( $1\ \text{mg}/\text{mL}$ ) was added. Cells were further incubated for  $3$  h before  $100\ \mu\text{L}$  of a solubilization solution ( $40\%$  DMF,  $16\%$  sodium dodecyl sulfate,  $2\%$  acetic acid,  $\text{pH} = 4.7$ ) was added to dissolve the generated formazan crystals. Finally, the absorbance was measured at  $\lambda = 570$  nm. The percentage of viable cells was determined by the absorbance of control groups of untreated cells, which was considered to represent  $100\%$  viability. Further controls were performed using  $0.3\%$  sodium dodecyl sulfate and a reference DON without DNP-ligands on the surface.

**Ligand Tracer Experiments.** For real-time binding studies using Ligand Tracer technology, a cell-culture treated  $2 \times 2$  multiwell Petri dish was coated with fibronectin to promote cell adherence.  $2$  mL of a fibronectin solution in PBS ( $c = 10\ \mu\text{g}/\text{mL}$ ) was transferred in each section of the multiwell Petri dish. The solution was incubated for  $1$  h at room temperature to allow fibronectin to bind to the dish surface. Cells were harvested, centrifuged, and resuspended at a cell density of  $0.8 \times 10^6$  cells/mL in RBL-2H3 culture medium. The fibronectin solution was removed from the multiwell dish, and  $3$  mL of the cell suspension was seeded in each section overnight at  $37\ ^\circ\text{C}$  and  $5\%$   $\text{CO}_2$ . On the next day, cells were washed twice with PBS buffer to remove dead and nonadhered cells. Subsequently, cells were sensitized with  $2$  mL of anti-DNP IgE ( $c = 1\ \mu\text{g}/\text{mL}$ ) in RBL-2H3 medium supplemented with  $1\ \text{mg}/\text{mL}$  BSA and incubated for  $1$  h to allow the binding of anti-DNP IgE to Fc $\epsilon$ RI. Each  $2 \times 2$  multiwell Petri dish was used to perform a technical duplicate with (+) and without (−) anti-DNP IgE for the binding of DNP-decorated DON to Fc $\epsilon$ RI-bound anti-DNP IgE and negative control, respectively. To remove the excess of antibodies in solution, cells were washed again with PBS and incubated for  $30$  min with poly inosinic acid (poly I,  $c = 40\ \mu\text{g}/\text{mL}$  in PBS,  $2$  mL/section) to saturate the scavenger receptor, responsible for uptaking polyanionic compounds like DNA-origami. Afterward, cells were washed with PBS, and  $1.5$  mL of culture medium supplemented with  $1\ \text{mg}/\text{mL}$  BSA was introduced to each connected chamber of two sections. All incubation steps were carried out in the cell incubator at a  $\text{CO}_2$  atmosphere of  $5\%$  and a temperature of  $37\ ^\circ\text{C}$  if not stated otherwise. The  $2 \times 2$  multiwell Petri dish was placed on a rotational support within the Ligand Tracer Green instrument (Ridgeview Instruments AB) equipped with a red (ex:  $632$  nm)–NIR (em:  $671$  nm) G2 fluorescence detector (Ridgeview Instruments AB), suitable for detecting Cy5. During measurements, the Petri dish was rotated inside the instrument, and the fluorescence was measured every  $72$  s with a detection time of  $15$  s at each position. The baseline measurement was conducted for  $20$  min before the instrument was opened and a Cy5-labeled DNP-decorated DON sample was introduced into the media of both chambers ( $c_{\text{final}} = 0.8$  nM). The association was measured for  $1$  h at room temperature before a higher concentration ( $c_{\text{final}} = 1.2$  nM) of the Cy5-labeled DNP-decorated DON was introduced for a second association phase of  $1$  h. Then, the analyte solution was removed and replaced by fresh culture medium without the analyte to measure dissociation for several hours. Measurements were conducted as technical duplicates and biological replicates (at least duplicates). To measure the binding kinetics of IgE to Fc $\epsilon$ RI expressed on the cell surface of RBL-2H3 cells, we labeled an anti-DNP IgE antibody with Cy5 fluorophores using a commercial conjugation kit (Abcam) according to manufacturer instructions. The experimental procedure was similar to that previously described above for the DNP-decorated DON, with the only difference that Cy5-labeled anti-DNP IgE was the analyte. Therefore, no incubation with poly-I was conducted beforehand and different analyte concentrations were used during association ( $c_1 = 2.5$  nM,  $c_2 = 5$  nM). Ligand Tracer sensorgrams were evaluated using TraceDrawer software (Ridgeview Instruments AB). Sensorgrams were signal corrected by subtraction of the sensorgrams obtained from the negative control. All sensorgrams were normalized and fitted in the same period to a 1:1 Langmuir binding model for kinetic analysis.

**Degranulation Assay.** For degranulation assays with RBL-2H3 cells, we coated Nunc MicroWell 96-Well Microplates (Invitrogen) with recombinant streptavidin<sup>71</sup> (Stv) for the immobilization of biotinylated capture oligonucleotides.  $50\ \mu\text{L}$  of Stv ( $200$  nM) in PBS buffer ( $137$  mM NaCl,  $2.7$  mM KCl,  $10$  mM  $\text{Na}_2\text{HPO}_4$ ,  $\text{KH}_2\text{PO}_4$ ,  $\text{pH} = 7.4$ ) was transferred into each well of the microplate. The plate was sealed with adhesive plate seals (Thermo Scientific) and incubated for  $72$  h at  $4\ ^\circ\text{C}$  on an orbital shaker. Afterward, microplates were washed three times for  $1$  min with TBS buffer ( $20$  mM Tris-Cl,  $150$  mM,  $\text{pH} = 7.35$ ). Each well was filled with  $150\ \mu\text{L}$  MESTBS buffer ( $20.0$  mmol/L Tris-Cl,  $150.0$  mmol/L NaCl,  $4.5\%$  milk powder,  $5.0$  mmol/L EDTA,  $1.0$  mg/mL herring sperm DNA (Promega),  $\text{pH} = 7.35$ ), the plate was sealed again and incubated for at least  $12$  h at  $4\ ^\circ\text{C}$ .

On the day of the experiment, wells were washed three times with TETBS buffer (20.0 mM Tris-Cl, 150.0 mM NaCl, 5.0 mM EDTA, 0.05% Tween-20, pH = 7.35). Afterward, 50  $\mu$ L of biotinylated capture oligonucleotides (Sigma, biotin-ATGATGATGATGATGATGATGATG) were transferred to each well, and the plate was incubated for 45 min on an orbital shaker at room temperature. The oligonucleotide solution was decanted, and the plate was washed two times with TETBS. To block free Stv binding sites, 240  $\mu$ L of TETBS buffer supplemented with d-biotin (800  $\mu$ M) was added to each well and incubated for 20 min. During this time, cells were prepared and sensitized. For this, RBL-2H3 cells were harvested, centrifuged, and resuspended in Tyrodes buffer (134 mM NaCl, 2.68 mM KCl, 1.8 mM CaCl<sub>2</sub>, 1.05 mM MgCl<sub>2</sub>, 0.42 mM NaH<sub>2</sub>PO<sub>4</sub>, 11.9 mM NaHCO<sub>3</sub>, 5.56 mM D-(+)-glucose, pH = 7.4) supplemented with 1 mg/mL BSA and 1  $\mu$ g/mL anti-DNP IgE at a cell density of  $1 \times 10^6$  cells/mL. Sensitization of cells was conducted for 1 h at 37 °C and 5% CO<sub>2</sub> atmosphere. Then, cells were centrifuged (1300g, 5 min, room temperature) and washed with 10 mL of PBS to remove an excess of unbound anti-DNP IgE. Cells were then resuspended at the desired cell density in Tyrodes buffer supplemented with 1 mg/mL BSA. For immobilization of the DON on the well surface, the plate was washed with TETBS buffer and DON samples were diluted with TeMg<sub>6</sub> mM buffer at different concentrations ( $c = 0.1$ – $5$  nM). 50  $\mu$ L of each dilution was transferred to the wells and incubated for 45 min at room temperature. After DON immobilization, the plate was washed with TETBS buffer, and  $4 \times 10^4$  cells were added to each well. The cells were then incubated on the DON-functionalized surface for 1 h in a cell incubator, and afterward, 25  $\mu$ L of the supernatant was transferred to another 96-well plate containing 1.2 mM of the substrate 4-methylumbelliferyl-N-acetyl- $\beta$ -D-glucosaminidase (MUG) in 50 mM sodium acetate buffer (pH = 4.4). Enzymatic reaction of the degranulated  $\beta$ -hexosaminidase was conducted for 30 min in the cell incubator and subsequently quenched by adding 175  $\mu$ L of 0.1 M glycine carbonate buffer (pH = 10). Fluorescent measurements of the hydrolyzed substrate were performed using a microplate reader Synergy H1 (BioTek) with excitation at  $\lambda = 360$  nm and emission at  $\lambda = 450$  nm. All measurements were performed in technical and biological triplicates. All washing steps were performed three times with 240  $\mu$ L per well and 5 min of incubation time on an orbital shaker, if not stated otherwise.

Stimulated degranulation of  $\beta$ -hexosaminidase was expressed as a percentage calculated from the maximal  $\beta$ -hexosaminidase activity in the lysate after cell solubilization in 0.1% Triton X-100. The amount of immobilized biotinylated capture oligonucleotides on the Stv-coated wells was quantified by a supernatant depletion assay. For this, Cy3-labeled oligonucleotides with the complementary sequence to the capture oligonucleotides were incubated on the surfaces at different concentrations (50 nM – 1  $\mu$ M) for 1 h at room temperature. The fluorescence (excitation at  $\lambda = 540$  nm and emission at  $\lambda = 570$  nm) was measured before and after hybridization using a microplate reader Synergy H1 (BioTek) to calculate the amount of hybridized, and thereby immobilized, oligonucleotides. To quantify the amount of immobilized DON, samples were taken from each DON dilution as well as from the supernatant of the wells for qPCR analysis.

## ASSOCIATED CONTENT

### Supporting Information

The Supporting Information is available free of charge at <https://pubs.acs.org/doi/10.1021/acsnano.2c12647>.

Structural information on DNP–DON design and assembly (Figures S1, S2, S9, and S10, Tables S5–S7), SPR sensorgrams of surface functionalization (Figure S3), SPR binding kinetics and kinetic evaluation of IgE and IgG to surface-immobilized DON (Figures S3–S5, Tables S1 and S2), Ligand Tracer binding kinetics of Fc $\epsilon$ RI-bound IgE to DNP–DON (Figures S6 and S12, Tables S3 and S4), quantification of immobilized

capture oligonucleotides and DNP–DON (Figure S7), degranulation assay of RBL-2H3 with DNP–DON M<sub>3</sub>, B<sub>6</sub>–B<sub>30</sub> and negative control (Figure S8), control experiments of degranulation assay of RBL-2H3 cells (Figure S11) (PDF)

## AUTHOR INFORMATION

### Corresponding Author

Christof M. Niemeyer – Institute of Biological Interfaces (IBG-1), Karlsruhe Institute of Technology (KIT), 76344 Eggenstein-Leopoldshafen, Germany; [orcid.org/0000-0002-8837-081X](https://orcid.org/0000-0002-8837-081X); Email: [niemeyer@kit.edu](mailto:niemeyer@kit.edu)

### Authors

Leonie Schneider – Institute of Biological Interfaces (IBG-1), Karlsruhe Institute of Technology (KIT), 76344 Eggenstein-Leopoldshafen, Germany; [orcid.org/0000-0002-3772-1480](https://orcid.org/0000-0002-3772-1480)

Kersten S. Rabe – Institute of Biological Interfaces (IBG-1), Karlsruhe Institute of Technology (KIT), 76344 Eggenstein-Leopoldshafen, Germany; [orcid.org/0000-0001-7909-8191](https://orcid.org/0000-0001-7909-8191)

Carmen M. Domínguez – Institute of Biological Interfaces (IBG-1), Karlsruhe Institute of Technology (KIT), 76344 Eggenstein-Leopoldshafen, Germany; [orcid.org/0000-0002-0918-5473](https://orcid.org/0000-0002-0918-5473)

Complete contact information is available at:

<https://pubs.acs.org/10.1021/acsnano.2c12647>

### Notes

The authors declare no competing financial interest.

## ACKNOWLEDGMENTS

This work was supported through the Helmholtz program “Materials Systems Engineering” under the topic “Adaptive and Bioinspired Materials Systems” and Deutsche Forschungsgemeinschaft (GRK 2039). Experimental assistance from S. Gimmel and S. Corbett is gratefully acknowledged. We further thank A. Descher and S. Bondza for their assistance with the evaluation of kinetic data and K. Potter and M. Sobol for proofreading of the manuscript.

## REFERENCES

- (1) Bachmann, M. F.; Jennings, G. T. Vaccine delivery: a matter of size, geometry, kinetics and molecular patterns. *Nat. Rev. Immunol.* **2010**, *10* (11), 787–796.
- (2) Jegerlehner, A.; Storni, T.; Lipowsky, G.; Schmid, M.; Pumpens, P.; Bachmann, M. F. Regulation of IgG antibody responses by epitope density and CD21-mediated costimulation. *Eur. J. Immunol.* **2002**, *32* (11), 3305–3314.
- (3) McAleer, W. J.; Buynak, E. B.; Maigetter, R. Z.; Wampler, D. E.; Miller, W. J.; Hilleman, M. R. Human hepatitis B vaccine from recombinant yeast. *Nature* **1984**, *307* (5947), 178–180.
- (4) Kirnbauer, R.; Booy, F.; Cheng, N.; Lowy, D. R.; Schiller, J. T. Papillomavirus L1 major capsid protein self-assembles into virus-like particles that are highly immunogenic. *Proc. Natl. Acad. Sci. U. S. A.* **1992**, *89* (24), 12180–4.
- (5) Wang, Y.; Baars, I.; Fördös, F.; Högberg, B. Clustering of Death Receptor for Apoptosis Using Nanoscale Patterns of Peptides. *ACS Nano* **2021**, *15* (6), 9614–9626.
- (6) Sibillano, R.; Frossi, B.; Pucillo, C. E. Mast cell activation: A complex interplay of positive and negative signaling pathways. *Eur. J. Immunol.* **2014**, *44* (9), 2558–2566.

- (7) Draber, P.; Halova, I.; Polakovcova, I.; Kawakami, T. Signal transduction and chemotaxis in mast cells. *Eur. J. Pharmacol.* **2016**, *778*, 11–23.
- (8) Gilmartin, L.; Tarleton, C. A.; Schuyler, M.; Wilson, B. S.; Oliver, J. M. A Comparison of Inflammatory Mediators Released by Basophils of Asthmatic and Control Subjects in Response to High-Affinity IgE Receptor Aggregation. *Int. Arch. Allergy Immunol.* **2008**, *145* (3), 182–192.
- (9) Mahajan, A.; Barua, D.; Cutler, P.; Lidke, D. S.; Espinoza, F. A.; Pehlke, C.; Grattan, R.; Kawakami, Y.; Tung, C.-S.; Bradbury, A. R. M.; Hlavacek, W. S.; Wilson, B. S. Optimal Aggregation of FcεRI with a Structurally Defined Trivalent Ligand Overrides Negative Regulation Driven by Phosphatases. *ACS Chem. Biol.* **2014**, *9* (7), 1508–1519.
- (10) Holowka, D.; Sil, D.; Torigoe, C.; Baird, B. Insights into immunoglobulin E receptor signaling from structurally defined ligands. *Immunol. Rev.* **2007**, *217* (1), 269–279.
- (11) Rashid, A.; Sadroddiny, E.; Ye, H. T.; Vratimos, A.; Sabban, S.; Carey, E.; Helm, B. Review: Diagnostic and therapeutic applications of rat basophilic leukemia cells. *Mol. Immunol.* **2012**, *52* (3), 224–228.
- (12) Liu, F. T.; Bohn, J. W.; Ferry, E. L.; Yamamoto, H.; Molinaro, C. A.; Sherman, L. A.; Klinman, N. R.; Katz, D. H. Monoclonal dinitrophenyl-specific murine IgE antibody: preparation, isolation, and characterization. *J. Immunol.* **1980**, *124* (6), 2728–2737.
- (13) Xu, K.; Goldstein, B.; Holowka, D.; Baird, B. Kinetics of multivalent antigen DNP-BSA binding to IgE-Fc epsilon RI in relationship to the stimulated tyrosine phosphorylation of Fc epsilon RI. *J. Immunol.* **1998**, *160* (7), 3225–35.
- (14) Gieras, A.; Linhart, B.; Roux, K. H.; Dutta, M.; Khodoun, M.; Zafred, D.; Cabauatan, C. R.; Lupinek, C.; Weber, M.; Focke-Tejkl, M.; Keller, W.; Finkelman, F. D.; Valenta, R. IgE epitope proximity determines immune complex shape and effector cell activation capacity. *J. Allergy Clin. Immunol.* **2016**, *137* (5), 1557–65.
- (15) Monine, M. I.; Posner, R. G.; Savage, P. B.; Faeder, J. R.; Hlavacek, W. S. Modeling multivalent ligand-receptor interactions with steric constraints on configurations of cell-surface receptor aggregates. *Biophys. J.* **2010**, *98* (1), 48–56.
- (16) Posner, R. G.; Subramanian, K.; Goldstein, B.; Thomas, J.; Feder, T.; Holowka, D.; Baird, B. Simultaneous cross-linking by two nontriggering bivalent ligands causes synergistic signaling of IgE Fc epsilon RI complexes. *J. Immunol.* **1995**, *155* (7), 3601–9.
- (17) Paar, J. M.; Harris, N. T.; Holowka, D.; Baird, B. Bivalent ligands with rigid double-stranded DNA spacers reveal structural constraints on signaling by Fc epsilon RI. *J. Immunol.* **2002**, *169* (2), 856–64.
- (18) Schweitzer-Stenner, R.; Licht, A.; Luescher, I.; Pecht, I. Oligomerization and ring closure of immunoglobulin E class antibodies by divalent haptens. *Biochemistry* **1987**, *26* (12), 3602–3612.
- (19) Baird, E. J.; Holowka, D.; Coates, G. W.; Baird, B. Highly Effective Poly(Ethylene Glycol) Architectures for Specific Inhibition of Immune Receptor Activation. *Biochemistry* **2003**, *42* (44), 12739–12748.
- (20) Sil, D.; Lee, J. B.; Luo, D.; Holowka, D.; Baird, B. Trivalent ligands with rigid DNA spacers reveal structural requirements for IgE receptor signaling in RBL mast cells. *ACS Chem. Biol.* **2007**, *2* (10), 674–84.
- (21) Rothmund, P. W. Folding DNA to create nanoscale shapes and patterns. *Nature* **2006**, *440* (7082), 297–302.
- (22) Shaw, A.; Lundin, V.; Petrova, E.; Fordos, F.; Benson, E.; Al-Amin, A.; Herland, A.; Blokzijl, A.; Hogberg, B.; Teixeira, A. I. Spatial control of membrane receptor function using ligand nanocalipers. *Nat. Methods* **2014**, *11* (8), 841–6.
- (23) Angelin, A.; Weigel, S.; Garrecht, R.; Meyer, R.; Bauer, J.; Kumar, R. K.; Hirtz, M.; Niemeyer, C. M. Multiscale Origami Structures as Interface for Cells. *Angew. Chem., Int. Ed. Engl.* **2015**, *54* (52), 15813–15817.
- (24) Huang, D.; Patel, K.; Perez-Garrido, S.; Marshall, J. F.; Palma, M. DNA Origami Nanoarrays for Multivalent Investigations of Cancer Cell Spreading with Nanoscale Spatial Resolution and Single-Molecule Control. *ACS Nano* **2019**, *13* (1), 728–736.
- (25) Hawkes, W.; Huang, D.; Reynolds, P.; Hammond, L.; Ward, M.; Gadegaard, N.; Marshall, J. F.; Iskratch, T.; Palma, M. Probing the nanoscale organisation and multivalency of cell surface receptors: DNA origami nanoarrays for cellular studies with single-molecule control. *Faraday Discuss.* **2019**, *219*, 203–219.
- (26) Veneziano, R.; Moyer, T. J.; Stone, M. B.; Wamhoff, E.-C.; Read, B. J.; Mukherjee, S.; Shepherd, T. R.; Das, J.; Schief, W. R.; Irvine, D. J.; Bathe, M. Role of nanoscale antigen organization on B-cell activation probed using DNA origami. *Nat. Nanotechnol.* **2020**, *15* (8), 716–723.
- (27) Hellmeier, J. P.; Platzer, R.; Karner, A.; Motsch, V.; Bamieh, V.; Preiner, J.; Brameshuber, M. O.; Stockinger, H.; Schütz, G. J.; Huppa, J. B.; Sevcsik, E. Spatial Requirements for T-Cell Receptor Triggering Probed via Functionalized DNA Origami Platforms. *Biophys. J.* **2020**, *118* (3), 245a.
- (28) Lanzerstorfer, P.; Muller, U.; Gordiyenko, K.; Weghuber, J.; Niemeyer, C. M. Highly Modular Protein Micropatterning Sheds Light on the Role of Clathrin-Mediated Endocytosis for the Quantitative Analysis of Protein-Protein Interactions in Live Cells. *Biomolecules* **2020**, *10* (4), 540.
- (29) Hellmeier, J.; Platzer, R.; Eklund, A. S.; Schlichthaerle, T.; Karner, A.; Motsch, V.; Schneider, M. C.; Kurz, E.; Bamieh, V.; Brameshuber, M.; Preiner, J.; Jungmann, R.; Stockinger, H.; Schütz, G. J.; Huppa, J. B.; Sevcsik, E. DNA origami demonstrate the unique stimulatory power of single pMHCs as T cell antigens. *Proc. Natl. Acad. Sci. U. S. A.* **2021**, *118* (4), e2016857118.
- (30) Fang, T.; Alvelid, J.; Spratt, J.; Ambrosetti, E.; Testa, I.; Teixeira, A. I. Spatial Regulation of T-Cell Signaling by Programmed Death-Ligand 1 on Wireframe DNA Origami Flat Sheets. *ACS Nano* **2021**, *15* (2), 3441–3452.
- (31) Berger, R. M. L.; Weck, J. M.; Kempe, S. M.; Hill, O.; Liedl, T.; Radler, J. O.; Monzel, C.; Heuer-Jungemann, A. Nanoscale FasL Organization on DNA Origami to Decipher Apoptosis Signal Activation in Cells. *Small* **2021**, *17* (26), 2101678.
- (32) Cremers, G. A. O.; Rosier, B. J. H. M.; Meijs, A.; Tito, N. B.; van Duijnhoven, S. M. J.; van Eenennaam, H.; Albertazzi, L.; de Greef, T. F. A. Determinants of Ligand-Functionalized DNA Nanostructure–Cell Interactions. *J. Am. Chem. Soc.* **2021**, *143* (27), 10131–10142.
- (33) Domínguez, C. M.; García-Chamé, M.; Müller, U.; Kraus, A.; Gordiyenko, K.; Itani, A.; Haschke, H.; Lanzerstorfer, P.; Rabe, K. S.; Niemeyer, C. M. Linker Engineering of Ligand-Decorated DNA Origami Nanostructures Affects Biological Activity. *Small* **2022**, *18* (35), 2202704.
- (34) Wang, M.; Yang, D.; Lu, Q.; Liu, L.; Cai, Z.; Wang, Y.; Wang, H.-H.; Wang, P.; Nie, Z. Spatially Reprogrammed Receptor Organization to Switch Cell Behavior Using a DNA Origami-Templated Aptamer Nanoarray. *Nano Lett.* **2022**, *22* (21), 8445–8454.
- (35) Frtús, A.; Smolková, B.; Uzhytchak, M.; Lunova, M.; Jirsa, M.; Henry, S. J. W.; Dejneka, A.; Stephanopoulos, N.; Lunov, O. The interactions between DNA nanostructures and cells: A critical overview from a cell biology perspective. *Acta Biomaterialia* **2022**, *146*, 10–22.
- (36) Morzy, D.; Bastings, M. Significance of Receptor Mobility in Multivalent Binding on Lipid Membranes. *Angew. Chem., Int. Ed.* **2022**, *61* (13), e202114167.
- (37) Shaw, A.; Hoffecker, I. T.; Smyrlaki, I.; Rosa, J.; Grevys, A.; Bratlie, D.; Sandlie, I.; Michaelsen, T. E.; Andersen, J. T.; Högberg, B. Binding to nanopatterned antigens is dominated by the spatial tolerance of antibodies. *Nat. Nanotechnol.* **2019**, *14* (2), 184–190.
- (38) Preiner, J.; Kodera, N.; Tang, J.; Ebner, A.; Brameshuber, M.; Blaas, D.; Gelbmann, N.; Gruber, H. J.; Ando, T.; Hinterdorfer, P. IgGs are made for walking on bacterial and viral surfaces. *Nat. Commun.* **2014**, *5* (1), 4394.

- (39) Sandin, S.; Ofverstedt, L. G.; Wikström, A. C.; Wrangle, O.; Skoglund, U. Structure and flexibility of individual immunoglobulin G molecules in solution. *Structure* **2004**, *12* (3), 409–15.
- (40) Sosnick, T. R.; Benjamin, D. C.; Novotny, J.; Seeger, P. A.; Trehwella, J. Distances between the antigen-binding sites of three murine antibody subclasses measured using neutron and x-ray scattering. *Biochemistry* **1992**, *31* (6), 1779–1786.
- (41) Sandin, S.; Öfverstedt, L.-G.; Wikström, A.-C.; Wrangle, Ö.; Skoglund, U. Structure and Flexibility of Individual Immunoglobulin G Molecules in Solution. *Structure* **2004**, *12* (3), 409–415.
- (42) Hewat, E. A.; Blaas, D. Structure of a neutralizing antibody bound bivalently to human rhinovirus 2. *EMBO J.* **1996**, *15* (7), 1515–1523.
- (43) Wan, T.; Beavil, R. L.; Fabiane, S. M.; Beavil, A. J.; Sohi, M. K.; Keown, M.; Young, R. J.; Henry, A. J.; Owens, R. J.; Gould, H. J.; Sutton, B. J. The crystal structure of IgE Fc reveals an asymmetrically bent conformation. *Nat. Immunol* **2002**, *3* (7), 681–686.
- (44) Wurzburg, B. A.; Jardetzky, T. S. Conformational Flexibility in Immunoglobulin E-Fc3–4 Revealed in Multiple Crystal Forms. *J. Mol. Biol.* **2009**, *393* (1), 176–190.
- (45) Holdom, M. D.; Davies, A. M.; Nettleship, J. E.; Bagby, S. C.; Dhaliwal, B.; Girardi, E.; Hunt, J.; Gould, H. J.; Beavil, A. J.; McDonnell, J. M.; Owens, R. J.; Sutton, B. J. Conformational changes in IgE contribute to its uniquely slow dissociation rate from receptor FcεRI. *Nat. Struct. Mol. Biol.* **2011**, *18* (5), 571–576.
- (46) Jensen, R. K.; Jabs, F.; Miehe, M.; Mølgaard, B.; Pfützer, W.; Möbs, C.; Spillner, E.; Andersen, G. R. Structure of intact IgE and the mechanism of ligelizumab revealed by electron microscopy. *Allergy* **2020**, *75* (8), 1956–1965.
- (47) Kanagaratham, C.; El Ansari, Y. S.; Lewis, O. L.; Oettgen, H. C., IgE and IgG Antibodies as Regulators of Mast Cell and Basophil Functions in Food Allergy. *Front. Immunol.* **2020**, *11*. DOI: 10.3389/fimmu.2020.603050
- (48) Bondza, S.; Stenberg, J.; Nestor, M.; Andersson, K.; Björkelund, H. Conjugation Effects on Antibody–Drug Conjugates: Evaluation of Interaction Kinetics in Real Time on Living Cells. *Mol. Pharmaceutics* **2014**, *11* (11), 4154–4163.
- (49) Turner, H.; Kinet, J.-P. Signalling through the high-affinity IgE receptor FcεRI. *Nature* **1999**, *402* (6760), 24–30.
- (50) Shin, J. S.; Greer, A. M. The role of FcεRI expressed in dendritic cells and monocytes. *Cell. Mol. Life Sci.* **2015**, *72* (12), 2349–60.
- (51) Menon, A. K.; Holowka, D.; Webb, W. W.; Baird, B. Cross-linking of receptor-bound IgE to aggregates larger than dimers leads to rapid immobilization. *J. Cell Biol.* **1986**, *102* (2), 541–550.
- (52) Bila, H.; Paloja, K.; Caroprese, V.; Kononenko, A.; Bastings, M. M. C. Multivalent Pattern Recognition through Control of Nano-Spacing in Low-Valency Super-Selective Materials. *J. Am. Chem. Soc.* **2022**, *144* (47), 21576–21586.
- (53) Chauhan, N.; Xiong, Y.; Ren, S.; Dwivedy, A.; Magazine, N.; Zhou, L.; Jin, X.; Zhang, T.; Cunningham, B. T.; Yao, S.; Huang, W.; Wang, X. Net-Shaped DNA Nanostructures Designed for Rapid/Sensitive Detection and Potential Inhibition of the SARS-CoV-2 Virus. *J. Am. Chem. Soc.* **2022**, DOI: 10.1021/jacs.2c04835.
- (54) Nagata, Y.; Suzuki, R. FcεRI: A Master Regulator of Mast Cell Functions. *Cells* **2022**, *11* (4), 622.
- (55) Naal, R. M. Z. G.; Tabb, J.; Holowka, D.; Baird, B. In situ measurement of degranulation as a biosensor based on RBL-2H3 mast cells. *Biosens. Bioelectron.* **2004**, *20* (4), 791–796.
- (56) Dráber, P.; Sulimenko, V.; Dráberová, E. Cytoskeleton in Mast Cell Signaling. *Front Immunol* **2012**, DOI: 10.3389/fimmu.2012.00130.
- (57) Azouz, N. P.; Matsui, T.; Fukuda, M.; Sagi-Eisenberg, R. Decoding the Regulation of Mast Cell Exocytosis by Networks of Rab GTPases. *J. Immunol* **2012**, *189* (5), 2169–2180.
- (58) Bucaite, G.; Kang-Pettinger, T.; Moreira, J.; Gould, H. J.; James, L. K.; Sutton, B. J.; McDonnell, J. M. Interplay between Affinity and Valency in Effector Cell Degranulation: A Model System with Polcalcin Allergens and Human Patient-Derived IgE Antibodies. *J. Immunol* **2019**, *203* (7), 1693–1700.
- (59) Joulia, R.; Gaudenzio, N.; Rodrigues, M.; Lopez, J.; Blanchard, N.; Valitutti, S.; Espinosa, E. Mast cells form antibody-dependent degranulatory synapse for dedicated secretion and defence. *Nat. Commun.* **2015**, *6* (1), 6174.
- (60) Wu, M.; Holowka, D.; Craighead, H. G.; Baird, B. Visualization of plasma membrane compartmentalization with patterned lipid bilayers. *Proc. Natl. Acad. Sci. U. S. A.* **2004**, *101* (38), 13798–803.
- (61) Suzuki, R.; Leach, S.; Liu, W.; Ralston, E.; Scheffel, J.; Zhang, W.; Lowell, C. A.; Rivera, J. Molecular editing of cellular responses by the high-affinity receptor for IgE. *Science* **2014**, *343* (6174), 1021–5.
- (62) Wu, M.; Baumgart, T.; Hammond, S.; Holowka, D.; Baird, B. Differential targeting of secretory lysosomes and recycling endosomes in mast cells revealed by patterned antigen arrays. *J. Cell Sci.* **2007**, *120* (17), 3147–3154.
- (63) Carroll-Portillo, A.; Spendier, K.; Pfeiffer, J.; Griffiths, G.; Li, H.; Lidke, K. A.; Oliver, J. M.; Lidke, D. S.; Thomas, J. L.; Wilson, B. S.; Timlin, J. A. Formation of a Mast Cell Synapse: FcεRI Membrane Dynamics upon Binding Mobile or Immobilized Ligands on Surfaces. *J. Immunol* **2010**, *184* (3), 1328–1338.
- (64) Sleytr, U. B.; Messner, P.; Pum, D.; Sára, M. Crystalline Bacterial Cell Surface Layers (S Layers): From Supramolecular Cell Structure to Biomimetics and Nanotechnology. *Angew. Chem., Int. Ed.* **1999**, *38* (8), 1034–1054.
- (65) Köhler, V. K.; Crescioli, S.; Fazekas-Singer, J.; Bax, H. J.; Hofer, G.; Pranger, C. L.; Hufnagl, K.; Bianchini, R.; Flicker, S.; Keller, W.; Karagiannis, S. N.; Jensen-Jarolim, E. Filling the Antibody Pipeline in Allergy: PIPE Cloning of IgE, IgG(1) and IgG(4) against the Major Birch Pollen Allergen Bet v 1. *Int. J. Mol. Sci.* **2020**, *21* (16), 5693.
- (66) Niemeyer, C. M. Semisynthetic DNA-Protein Conjugates for Biosensing and Nanofabrication. *Angew. Chem., Int. Ed. Engl.* **2010**, *49* (7), 1200–1216.
- (67) Li, J.; Pei, H.; Zhu, B.; Liang, L.; Wei, M.; He, Y.; Chen, N.; Li, D.; Huang, Q.; Fan, C. Self-Assembled Multivalent DNA Nanostructures for Noninvasive Intracellular Delivery of Immunostimulatory CpG Oligonucleotides. *ACS Nano* **2011**, *5* (11), 8783–8789.
- (68) Vogele, K.; List, J.; Simmel, F. C.; Pirzer, T. Enhanced Efficiency of an Enzyme Cascade on DNA-Activated Silica Surfaces. *Langmuir* **2018**, *34* (49), 14780–14786.
- (69) Stahl, E.; Martin, T. G.; Praetorius, F.; Dietz, H. Facile and scalable preparation of pure and dense DNA origami solutions. *Angew. Chem., Int. Ed. Engl.* **2014**, *53* (47), 12735–40.
- (70) Mosmann, T. Rapid colorimetric assay for cellular growth and survival: Application to proliferation and cytotoxicity assays. *J. Immunol Methods* **1983**, *65* (1), 55–63.
- (71) Schmidt, T. G. M.; Skerra, A. One-step affinity purification of bacterially produced proteins by means of the “Strep tag” and immobilized recombinant core streptavidin. *J. Chromatography A* **1994**, *676*, 337–345.